





First-principles investigation of the impact of stress and lattice vibration on the hyperfine interactions of the nitrogen-vacancy center in diamond

Mingzhe Liu ^{1,2}, Xin Zhao ^{1,2}, Tianyu Xie ^{1,2}, Shaoyi Xu,^{1,2} Fazhan Shi,^{1,2,3,4,*} and Chang-Kui Duan ^{1,2,3,†}

¹CAS Key Laboratory of Microscale Magnetic Resonance and School of Physical Sciences,
University of Science and Technology of China, Hefei 230026, China

²CAS Center for Excellence in Quantum Information and Quantum Physics,
University of Science and Technology of China, Hefei 230026, China

³Hefei National Laboratory, University of Science and Technology of China, Hefei 230088, China

⁴School of Biomedical Engineering and Suzhou Institute for Advanced Research,
University of Science and Technology of China, Suzhou 215123, China



(Received 1 August 2023; accepted 13 October 2023; published 30 October 2023)

The hyperfine interactions between the electronic spin of the nitrogen-vacancy (NV) center in diamond and its surrounding nuclear spins are essential for quantum sensing and information processing. However, these interactions can be influenced by strains and lattice vibrations, causing changes in the resonant frequencies and thus the decoherence of multispin system. We used first-principles calculations to obtain the linear response of the hyperfine tensors to all the independent strain components and then converted it to stress response using the elastic tensor, which was obtained via first principles calculation as well. Additionally, we obtained the thermal expansion relation $V(T, P)$ for the NV center from first-principles calculations, rather than relying on experimental data for pristine diamond. This enabled us to calculate the hyperfine tensors as a function of thermal state variables T and P , i.e., $A(T, P)$, with the previously overlooked volume-dependence of the vibrational contribution included. For the ^{14}N nucleus, the hyperfine interaction variation is mainly due to the vibrational contribution A_{ph} , which is insensitive to volume changes due to the near cancellation of two volume-dependent terms. For the surrounding ^{13}C nuclei, our calculations confirm previous findings that both the change of the static term A_0 by thermal expansion and the vibration term A_{ph} are important. Our results reveal a complex interplay among structural, electronic, and vibrational properties of the NV center system and present a comprehensive method for calculating small variations of physical quantities due to external perturbation.

DOI: [10.1103/PhysRevB.108.155150](https://doi.org/10.1103/PhysRevB.108.155150)

I. INTRODUCTION

Detailed understanding of the properties of spin defects in solids [1] is essential in developing and optimizing their applications in quantum sensing [2], quantum computation and networks [3]. Measuring the susceptibilities of target defects to external perturbations such as magnetic fields, electric fields, strains and temperature enables detection of these quantities and analysis of decoherence resulting from their fluctuations. As one of the most prominent systems with its various properties carefully investigated [4], nitrogen-vacancy (NV) center in diamond has achieved several remarkable milestones including single-molecule magnetic resonance [5–7], nanoscale magnetic [8–10] and temperature [11,12] imaging, and multinode quantum networks [13,14]. However, the properties of NV centers are subject to the influence of environment, including temperature and stress, especially for nanoparticles [11,12,15]. This can affect their performance in quantum sensing and information processing applications. As such, it is important to investigate how these external factors

influence the spin-spin interactions in NV centers. One key parameter that characterizes these interactions is the zero-field splitting (ZFS), whose temperature and pressure dependencies have been explored theoretically in previous works [16,17]. Other important parameters are related to the hyperfine interaction, which arises from the coupling of the electron spin of the NV center with the nuclear spins of the surrounding atoms, such as ^{14}N and ^{13}C . The hyperfine interaction can be used to perform quantum operations such as initialization, readout, and entanglement of nuclear spins. It consists of both isotropic and anisotropic terms, which depend on the electron spin density distribution and the relative orientation of the electron and nuclear magnetic moments [18,19].

Currently, it is still challenging to resolve experimentally all individual components of the hyperfine couplings, particularly in the presence of strain or stress or at finite temperatures. First-principles calculations based on density functional theory (DFT) provide a valuable tool to obtain the quantum mechanical spin-spin interactions for nuclei at 0 K. To extend these calculations to the cases of finite temperatures or applied stress, the vibrational contribution to the thermodynamics and the perturbation of the ground-state wave function need to be taken into account. In our previous work [20], we measured the temperature-dependent hyperfine couplings of NV

*fzshi@ustc.edu.cn

†ckduan@ustc.edu.cn

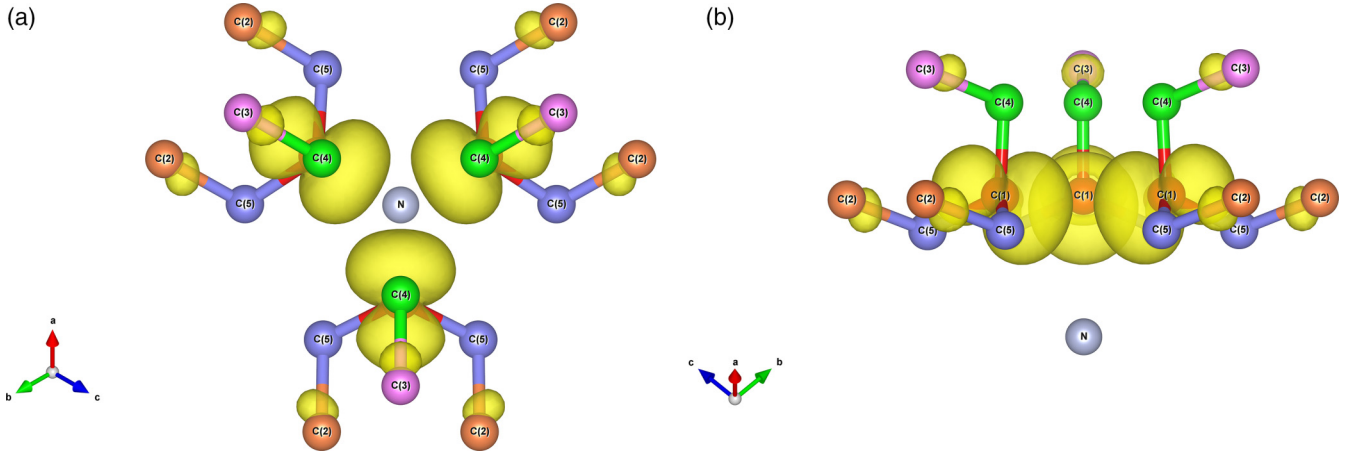


FIG. 1. The illustration of the nuclei around NV center with the spin density function contour via (a) top view and (b) front view. The ^{14}N and $^{13}\text{C}(1-5)$ nuclei equivalent by symmetry are marked in same color.

centers in diamond at room temperature with high precision. We demonstrated the feasibility of describing the temperature variation of hyperfine interactions by first-principles calculations with a rough model. In this work, we study how stress affects the hyperfine interactions and how thermal expansion modifies the vibrational contribution of the hyperfine interactions. We use first-principles calculations to obtain the linear response of the hyperfine tensors to normal and shear stress components. Furthermore, we calculate the thermal expansion relation $V(T, P)$ for the NV center instead of relying on the experimental data for perfect diamond like previous works [17,20,21]. This allows us to determine the hyperfine tensors $A(T, P)$ for varying pressure by including the previously overlooked volume-dependence of the vibrational contribution.

This work focuses on several important sites of nuclear spins surrounding the NV center in diamond, as shown in Fig. 1. The NV center is a point defect in the diamond lattice, made up of a nitrogen atom and an adjacent vacancy. Its ground state is a spin triplet, which can be optically initialized and read out. The electronic spin of the NV center interacts with the nuclear spins of the nitrogen and several carbon atoms near the defect through hyperfine coupling. Due to the C_{3v} symmetry of the NV center, some nuclear sites are equivalent and only one representative site for each symmetry class is considered. The properties of other nuclei can be obtained from those of the representative ones simply by coordinate transformations.

II. THEORETICAL FRAMEWORK

For a macroscopic physical quantity A determined by the thermal equilibrium properties of the solids, $A(T, P)$, we can also express A as a function of temperature and volume for the ease of computation, as it is more convenient to deal with the electron-phonon system at a series of volumes than pressures in actual calculation. Assuming no phase transition occurs in the range of solid states we consider, the function $A(T, P) = A(T, V(T, P))$ should be smooth.

Microscopically, the hyperfine couplings of the NV center in diamond are dependent on the structural configuration of the system that specifies the atomic positions and the

electronic spin density. The instantaneous values of those quantities fluctuate along the motion of atoms in the solids. We need to focus on their ensemble average in a time interval of the nanosecond scale, which is longer than in orders of magnitudes that the time scale of the motion of electrons and lattice vibrations in thermal equilibrium. We use the variation of phonon population to describe the atomic motions at finite temperature with the harmonic approximation. The phonon energy is much larger than the hyperfine coupling, with a difference in orders of magnitude of 10 THz versus 10 MHz. This implies that the lattice vibrations evolve much faster than the hyperfine couplings between the nuclear spins and electronic spins, let alone the much larger energy scale of electronic motions. We employ a Born-Oppenheimer-like approximation [22] to separate the motions of vibration and nucleus spins under hyperfine interactions, while neglecting the impact of the hyperfine interaction on electron and phonon states. We assume that lattice vibrations are always in thermal equilibrium when measuring the hyperfine parameter, and that the hyperfine parameter can be averaged over the thermal equilibrium distribution of lattice vibrations.

For a specific geometric configuration of all the nuclei, the hyperfine tensor can be expressed as the sum of an isotropic part (the Fermi contact term) and an anisotropic part as follows:

$$(\mathbf{A}_{\text{iso}}^I)_{ij} = \frac{2}{3} \frac{\mu_0 \gamma_e \gamma_I}{\langle S_z \rangle} \delta_{ij} \int \delta_T(\mathbf{r}) \rho_s(\mathbf{r} + \mathbf{R}_I) d\mathbf{r}, \quad (1)$$

$$(\mathbf{A}_{\text{ani}}^I)_{ij} = \frac{\mu_0 \gamma_e \gamma_I}{4\pi \langle S_z \rangle} \int \frac{\rho_s(\mathbf{r} + \mathbf{R}_I)}{r^3} \frac{3r_i r_j - \delta_{ij} r^2}{r^2} d\mathbf{r}, \quad (2)$$

where ρ_s is the spin density, μ_0 is the magnetic susceptibility of free space, γ_e the electron gyromagnetic ratio, γ_I the nuclear gyromagnetic ratio of the nucleus at \mathbf{R}_I , and $\langle S_z \rangle$ the expectation value of the z component of the total electronic spin. r_i is the i th component of \mathbf{r} , and \mathbf{r} is taken relative to the position of the nucleus \mathbf{R}_I . $\delta_T(r)$ is a smeared out δ function [23–25]. We do not include the contribution from electron angular momentum in the anisotropic part. This is because the spin-orbit coupling is deemed insignificant and

thus overlooked, leading to such a contribution being zero [24].

The Fermi contact term represents the magnetic interaction between an electron and an atomic nucleus, which depends on the value of the electron wave function at the nucleus. This term is responsible for the appearance of isotropic hyperfine coupling and is independent of orientation. The anisotropic term of hyperfine coupling arises from dipole coupling between the electron and nuclear magnetic moments, reflecting the spatial distribution of the electron spin density around the nucleus. This term can be described by a 3×3 tensor that has three diagonal and three off-diagonal independent elements.

A. The thermal equilibrium state of diamond

The relation $V(T, P)$ can be obtained either through experimental measurement or by fitting it to the equation of state after computing the thermodynamic functions of the solid, as we do in this work. All these parameters are determined from the free energy $F[T, V]$ using first-principle calculations. Generally, the free energy $F[T, V]$ can be estimated by the ground state energy $E_{\text{grd}}[V]$, and the temperature related contributions due to electron excitation $F^{\text{el}}[T, V]$ and lattice vibrations $F^{\text{ph}}[T, V]$ [26]. For diamond at least in the temperature range of 0–500 K, the electronic contribution to the free energy, $F^{\text{el}}[T, V]$, and the anharmonic phonon contribution are negligible and are therefore ignored here. The phonon contribution to the free energy $F^{\text{ph}}[T, V]$, can then be approximated by the quasiharmonic approximation as $F^{\text{qh}}[T, V]$. The expression for $F[T, V]$ is given as follows [27]:

$$\begin{aligned} F[T, V] &= E_{\text{grd}}[V] + F^{\text{qh}}[T, V] \\ &= E_{\text{grd}}[V] + \sum_{i=1}^{3N-3} \left\{ \frac{\hbar\omega_i[V]}{2} \right. \\ &\quad \left. + k_B T \ln \left[1 - \exp \left(-\frac{\hbar\omega_i[V]}{k_B T} \right) \right] \right\}, \end{aligned} \quad (3)$$

where the constant \hbar is the reduced Planck constant, k_B is the Boltzmann constant, N represents the number of atoms in the supercell, and ω_i is the frequency of the i th phonon mode, with the three translation degrees of freedom excluded. For insulators, the electronic term $F^{\text{el}}[T, V]$ in Eq. (3) is neglected, and the phonon term $F^{\text{ph}}[T, V]$ is given explicitly under the quasiharmonic approximation [28].

The state-parameter relationship $V(T, P)$ is determined by the equilibrium state of the system obtained from Eq. (4) by setting $P = -(\partial F / \partial V)_T$. Figure 2(a) shows the procedure for actual first-principles calculations, where a series of V values are artificially chosen and $F[T, V]$ is obtained via Eq. (4) for any given T_j . A smooth $F[T_j, V] \sim V$ curve can be determined by fitting F as a function of V . The equilibrium volume under condition (P_i, T_j) is then obtained by finding the volume that satisfies $\partial F / \partial V = -P_i$ from the $F[T_j, V] \sim V$ curve, which corresponds to the $V(T)$ relationship at a specific P_i . It should be noted that even at 0 K, where the phonon number is zero, vibrations have an impact on the equilibrium lattice parameters due to zero-point vibration, resulting in an expansion of the lattice over the classical value obtained by the energy minimum of about 0.37 % for diamond.

At typical temperatures of interest, thermal expansion can be neglected compared to the elastic deformation of the lattice. The P - V relationship, or more generally, the σ - ε relationship, can be obtained from first-principles calculations using either a finite differences approach [31] or density-functional-perturbation theory. In the linear response region, this relationship is given by

$$\sigma_i = \sum_j E_{ij} \cdot \varepsilon_j, \quad (5)$$

where stress σ (with σ_i its component) and strain ε (with ε_j its component) are symmetric rank-2 tensors with six independent components and are usually expressed as six-dimensional vectors that include normal and shear components. The rank-4 elastic tensor \mathbf{E} is typically written as a 6×6 matrix with up to 21 independent components E_{ij} , reflecting the symmetry and anisotropy of the material. The detailed form of Eq. (5) for the NV center is given in Appendix B. We can compare the $P \sim V$ relationship from the generalized Hooke's law with the classical $P(V)$ that neglects the phonon term in Eq. (4), and evaluate the accuracy of the equation of state for describing the elastic properties of the solid.

B. The temperature and pressure dependencies of hyperfine interactions

To conveniently describe the variation of hyperfine coupling from various factors, $\mathbf{A}(T, V(T, P))$ is divided into two parts as follows:

$$\mathbf{A}(T, V(T, P)) = \mathbf{A}_0(V(T, P)) + \mathbf{A}_{\text{ph}}(T, V(T, P)), \quad (6)$$

$$\mathbf{A}_0(V) = \mathbf{A}_0(V_0) + [\mathbf{A}_0(V) - \mathbf{A}_0(V_0)], \quad (7)$$

$$\mathbf{A}_{\text{ph}}(T, V) = \mathbf{A}(T, V) - \mathbf{A}_0(V), \quad (8)$$

where $\mathbf{A}_0(V)$ denotes the static hyperfine coupling that depends only on the lattice volume and the vibrational contribution part $\mathbf{A}_{\text{ph}}(T, V)$ arises from the statistical contribution of nuclei vibrations at temperature T and specific volume V . V_0 represents a reference volume, which is usually taken as the classical equilibrium volume of minimal vibration potential energy or the total energy of the first-principles calculation. It should be noted that $\mathbf{A}_0(V)$ differs from $\mathbf{A}(0, V)$ by $\mathbf{A}_{\text{ph}}(0, V)$, which is not zero due to zero-point vibration.

The hyperfine parameter $\mathbf{A}_0(V)$ can be further divided into several components based on the cause of volume change. This includes the hyperfine parameter at a standard volume V_0 , the change in hyperfine interaction due to mechanical volume change $\mathbf{A}_0(V(0, P)) - \mathbf{A}_0(V_0)$, and the change in hyperfine interaction due to thermal expansion $\mathbf{A}_0(V(T, P)) - \mathbf{A}_0(V(0, P))$. In this context, V_0 is considered as $V(0, 0)$, which is the equilibrium volume without external pressure at 0 K. If we only consider a small range of lattice shape changes, $\mathbf{A}_0(V)$ will have a linear relationship with volume [20]. The volume-induced variation of hyperfine coupling can be approximated as the linear coefficient $d\mathbf{A}_0/dV$ multiplied by the volume changes, which can be obtained from $V(T, P)$ in the previous section.

For realistic anisotropic mechanical cases, the volume and pressure in Eq. (8) can be generalized to strain and stress

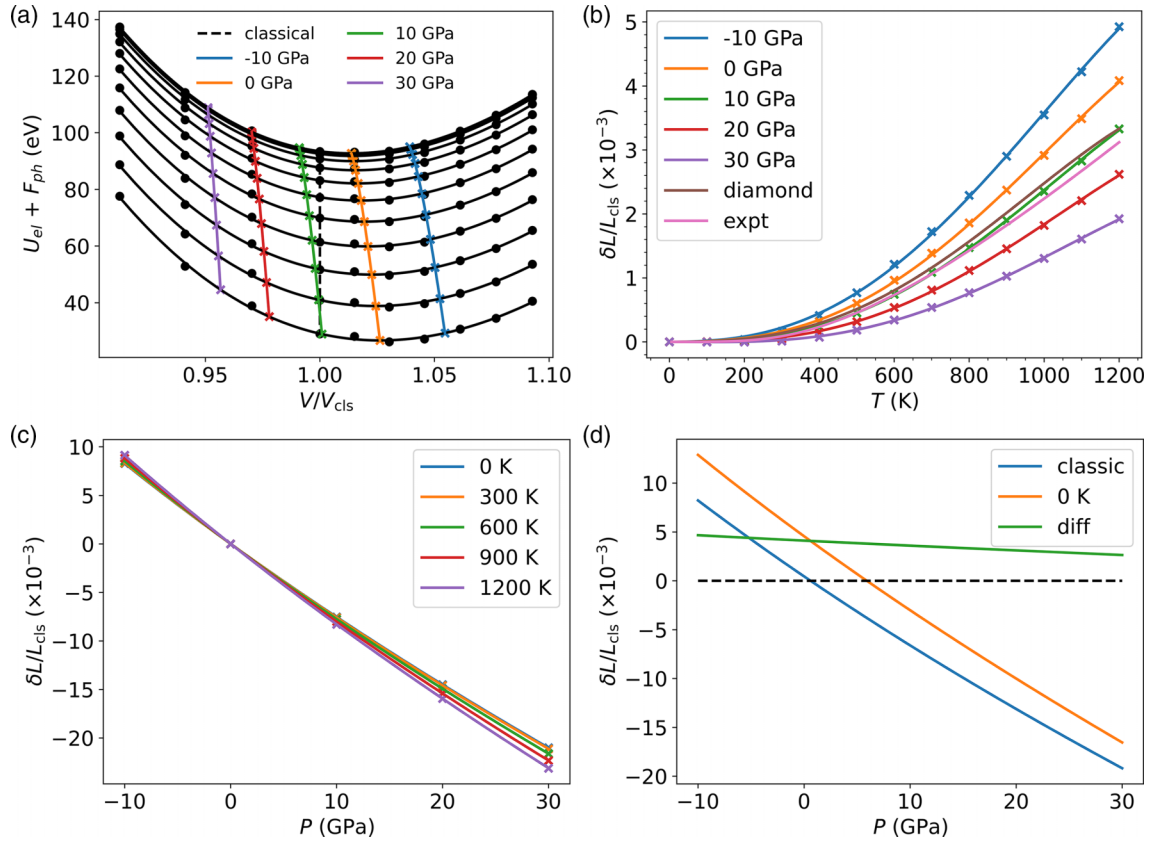


FIG. 2. For diamond with an NV center, (a) the free energy of $F(T, V)$ calculated with Eq. (4), (b) the temperature dependent lattice scale factor $\delta L(T)|_P/L_{\text{cls}}(0)$ under various pressures, (c) the pressure dependent lattice scale factor $\delta L(T)|_P/L_{\text{cls}}(0)$ under various temperatures, and (d) the pressure dependence of the zero-point vibrational contribution on lattice expansion. For convenience, the uniform lattice strain is described by the scale factor $(\delta L/L)$ instead of volume in actual calculations. In (a), the black points are temperature and volume samples; the black curves specify $F(V)$ from 0 to 1200 K with a step of 100 K and the free energy are fitted by the third-order Birch-Murnaghan equation [29]; the vertical dashed line marks the classical volume under no external pressure $V_{\text{cls}}(0)$ and the color lines represent the $V(T, P)$'s. In (b), “diamond” is the case pristine diamond under no external pressure; “expt” is the experimental curve of diamond fitted by the multifrequency Einstein model in a wide range of temperatures T [30].

tensors, respectively. Due to the high degree of freedom of strain ε and stress σ , we simplify the problem by not considering $\varepsilon(\sigma, T)$ in calculating A_0 together with A_{ph} . We separately consider the case of anisotropic stress when the temperature effect is neglected, i.e., A_0 without including A_{ph} , and the case of finite temperature with only hydrostatic pressure for A_0 and A_{ph} .

At a specific volume V , the $A_{\text{ph}}(T, V)$ term is handled using the frozen-phonon method [32]. This method calculates the parameters of nuclear spin evolution when atomic displacements are frozen in both time and space. A physical quantity $A_0(\{X_i\}, V)$ with displacement $\{\delta X_i\}$ can be expanded to the second order in δX_i as follows:

$$\begin{aligned}
 A_0(\{\delta X_i\}, V) &= A_0(V) + \sum_i \frac{\partial A_0}{\partial X_i} \delta X_i \\
 &+ \frac{1}{2} \sum_i \frac{\partial^2 A_0}{\partial X_i^2} (\delta X_i)^2 + \sum_{i < j} \frac{\partial^2 A_0}{\partial X_i \partial X_j} \delta X_i \delta X_j \\
 &+ \dots
 \end{aligned} \tag{9}$$

The hyperfine parameter $A(T, V)$ is then an ensemble average of $A(\{\delta X_i\}, V)$ at temperature T , where $\{\delta X_i\}$ are the normal

coordinates of the i th phonon mode. The form of $A_{\text{ph}}(T, V)$ could be further given as follows:

$$A_{\text{ph}}(T, V) = A(T, V) - A_0(V) \tag{10}$$

$$= \frac{1}{2} \sum_i \frac{\partial^2 A_0}{\partial X_i^2}(V) \frac{\hbar}{\omega_i(V)} \left(\langle n_i \rangle_T + \frac{1}{2} \right) \tag{11}$$

$$= \sum_i c_i \left(\langle n_i \rangle_T + \frac{1}{2} \right). \tag{12}$$

Here, $\langle n_i \rangle_T = [\exp(\hbar\omega_i(V)/k_B T) - 1]^{-1}$ is the expectation phonon number of mode i at temperature T , k_B the Boltzmann constant, with ω_i the phonon frequency of the i th vibration mode and \hbar the reduced Planck's constant. Within quasiharmonic approximation, the linear $\langle X_i \rangle_T$ and cross $\langle X_i X_j \rangle_T$ terms are zero and the diagonal second-order term in Eq. (9) can be evaluated via $\langle X_i^2 \rangle_T = (\langle n_i \rangle_T + 1/2)\hbar/\omega_i$. The mode-wise term $c_i = \partial^2 A_0 / \partial X_i^2 \hbar / (2\omega_i)$ as the thermodynamic contribution on hyperfine interaction for one phonon of mode i . The diagonal second-order coefficients $\partial^2 A_0 / \partial X_i^2$ can be obtained by finite-difference in standard frozen-phonon method or fitting the $A_0(X_i)$ with a quadratic

curve for any given i by first-principles calculation. It is more complicated and will be avoided to obtain accurately the nondiagonal second-order coefficients. We also noted that the zero-point vibration not only has a contribution on lattice strain but also has an effect on A_{ph} , which equals to $c_i/2 = \sum_i (\partial^2 A_0(\mathbf{X}_i, \mathbf{V}) / \partial X_i^2) \hbar / (4\omega_i(V))$.

The vibrational contribution term, $A_{\text{ph}}(T, V)$, is dependent on both temperature T and volume V . The volume change has a weak effect on the phonon modes in terms of frequencies and atomic motions. To determine the volume dependence of $A_{\text{ph}}(T, V)$, it is necessary to know the second-order coefficient $\partial^2 A_0 / \partial X_i^2$ as a function of volume and the volume-dependent phonon frequencies. The weak volume dependence was neglected in our previous work [20].

C. Computational details

The electronic and phonon calculations were carried out with the projector augmented wave method [33] and finite differences approach implemented in the Vienna *ab initio* simulation package code (VASP) [34,35], respectively. The hyperfine tensors for nuclei are calculated with Eq. (2) implanted in VASP, and the core electronic contributions to the Fermi contact term are calculated in the frozen valence approximation as proposed by [25]. The supercells containing $4 \times 4 \times 4$ of the diamond's unit cell are adopted to represent an isolated NV⁻ center in diamond which is large enough for phonon and hyperfine coupling calculation (see Fig. S1 for the comparison between two supercells with different sizes). To balance accuracy and computational cost, the lattice vibration of the supercell at the Γ point are calculated with the PBEsol (PBE for solids) density functional [36] and a 520 eV energy cutoff to decrease the effect of "Pulay pressure" [37]. The nuclear gyromagnetic ratios of ¹⁴N and ¹³C nuclei are from Ref. [38].

One of the factors that may affect the vibrational properties of diamond is the presence of ¹³C isotopes, which have a larger mass than the more abundant ¹²C isotopes. However, previous studies have shown that the mass difference has a negligible impact on the phonon properties of the supercell [39,40], and no effect on the spin density. Therefore, in our practical calculations, we neglect the mass difference between ¹³C and ¹²C isotopes, and treat all the carbon nuclei as ¹²C. This approximation allows us to consider the vibrational modes of the system in a single calculation, which simplifies the problem and reduces the computational cost.

III. RESULT AND DISCUSSION

We present the results on the static hyperfine interaction A_0 and its dependence on the volume $V(T, P)$, or more generally, on the strain. Then, the vibrational contributions to hyperfine interaction A_{ph} as a function of temperature and pressure via the thermal equilibrium state $V(T, P)$ were evaluated and the hyperfine tensor $A(T, P)$ and its responses to temperature and pressured are discussed.

The static term A_0 is achieved in actual calculation by

$$A_0(V) \approx A_0(V_{\text{cls}}(0)) + \frac{dA_0}{dV} [V(T, P) - V_{\text{cls}}(0)], \quad (13)$$

where $V_{\text{cls}}(P)$ refers to the classical equilibrium volume under a certain pressure which ignores all the vibration effect, so it is only related to the pressure. The actual volume $V(T, P)$ can be divided into four components by different contributions: the classical volume at zero external pressure $V_{\text{cls}}(0)$, the variations induced by pressure $V_{\text{cls}}(P) - V_{\text{cls}}(0)$, the thermal expansion $V(T, P) - V(0, P)$ and the zero-point vibration $V(0, P) - V_{\text{cls}}(P)$. The thermal expansion and the changes of volume under pressure of interest in this work are much smaller than the value $V_{\text{cls}}(0)$ or $V(0, 0)$, so that the linear approximation in Eq. (13) holds.

By applying Eq. (2) to the equilibrium geometry of the supercell, determined by energy minimization, we obtain the hyperfine tensors $A(0, V_{\text{cls}}(0))$ for the nuclei surrounding the NV center. The results are given in Appendix B. The NV center reduces the original site symmetry of point group T_d to C_{3v} . We choose a coordinate system such that the x , y , and z axes are along (100), (010), and (001), respectively, with the $\langle C_3 \rangle$ axis along (111). The isotropic Fermi contact term dominates these tensors, resulting in much larger diagonal values than off-diagonal ones. To clearly illustrate and compare with experimental measurements [20], we focus on the following parameter:

$$A = \text{sgn}(\mathbf{n} \cdot \mathbf{A} \cdot \mathbf{n}) |\mathbf{n} \cdot \mathbf{A}|, \quad (14)$$

where $\mathbf{n} = \sqrt{1/3}(1, 1, 1)$ is the principal axis of the single NV center and the function $\text{sgn}(\dots)$ is to take the sign. The hyperfine parameters $A(0, V_{\text{cls}}(0))$ for ¹⁴N and ¹³C(1-5) in MHz are respectively $-1.6936(4)$, $128.18(3)$, $14.851(1)$, $13.918(1)$, $-7.0160(5)$, and $-5.652(2)$, which are almost the same with our previous results [20] obtained with a different density functional setting.

A. Static hyperfine interaction and lattice strain

Due to the high degree of freedom when applying strain to the diamond lattice, we try to avoid considering both strain and temperature effects simultaneously. According to the $V(T, P)$ obtained below, for the range of temperatures and stress ranges we are interested in, the thermal effect is found to be less important for the diamond lattice. By neglecting thermal expansion, the pressure-induced volume variation $V_{\text{cls}}(P) - V_{\text{cls}}(0)$ or its generalized form $\epsilon_{\text{cls}}(\sigma) - \epsilon_{\text{cls}}(0)$ can be derived using classical mechanical calculations with Eq. (5). The strain and stress are related by the elastic tensor [41] as shown in Eq. (B1). For the independent elements in the elastic tensor of pristine diamond under no external stress, C_{11} , C_{12} and C_{44} are respectively calculated to be 1080, 142, and 581 GPa, comparable with the measured values of 1079, 124, and 578 GPa for perfect diamond [42]. The other terms are zero due to the crystallographic point group of O_h . For diamond with an NV center, C_{11} , C_{12} , and C_{44} show a linear dependence on volume and the other three C_{45} , C_{15} , and C_{14} are below the accuracy limit of the calculations. Their values at V_{cls} can be found in Appendix B.

The strain-dependence of hyperfine parameters $A_0(\epsilon)$ are acquired by linear fitting of calculated hyperfine tensors and calculated using Eq. (14) (details can be referred to Figs. S2

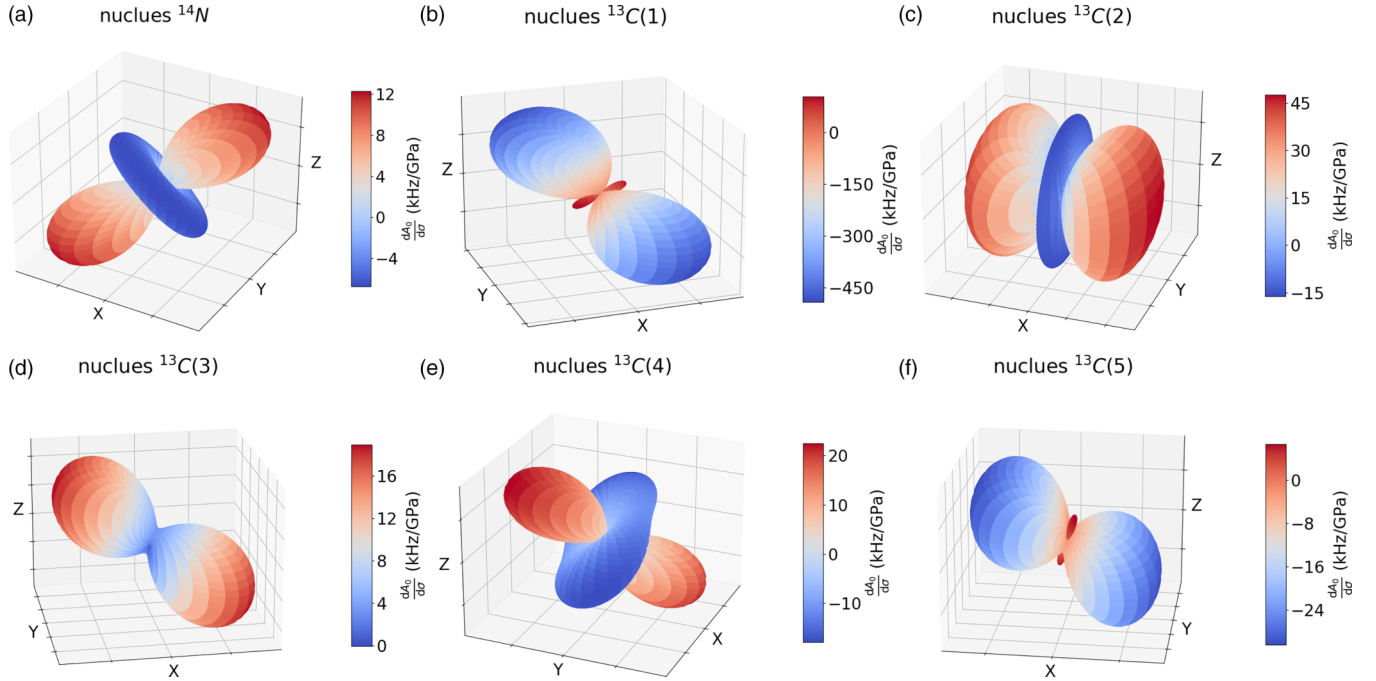


FIG. 3. The stress orientation dependence of hyperfine parameter derivative $dA_0/d\sigma$ of (a) ^{14}N and (b)–(f) ^{13}C nuclei.

and S3 in Ref. [43], which contains [20,44]), and their strain derivatives $\partial A_0/\partial \epsilon$ can be found in Appendix C, which indicates that our calculations respect the symmetry constraints automatically. It is noted that the strains not along the $\langle C_3 \rangle$ axis break the C_{3v} symmetry and cause the hyperfine parameters of the originally equivalent nuclei to differ. According to Appendix C, the hyperfine parameter on ^{14}N nucleus is more sensitive to the shear strains than to the normal strains, on the contrary, the hyperfine parameter on $^{13}\text{C}(2)$ nucleus is more sensitive to normal strains. For the rest of the nuclei, their hyperfine parameter responses to normal strains and shear strains are comparable.

The linear relationship between hyperfine parameters and strains results in the additivity of the hyperfine parameter variations on strains. As shown in Table S1 in Ref. [43], the verification is successful, with deviations mostly less than 10%, except when values are very small. Figure 3 shows the variations of hyperfine parameters under stress in all directions. The derivative $dA_0/d\sigma$ of the ^{14}N nucleus has a rotation axis that coincides with the $\langle C_3 \rangle$ axis. Under normal stress along x , y or z axis, the hyperfine coupling barely reacts, while for normal stress along $1/\sqrt{3}(111)$, i.e., $(1/\sqrt{3}, 1/\sqrt{3}, 1/\sqrt{3})^T(1/\sqrt{3}, 1/\sqrt{3}, 1/\sqrt{3}) = 1/3(111; 111; 111)$ in the same coordinate (superscript “ T ” denoting transposition), the derivative $dA_0/d\sigma$ reaches the maximum since the hyperfine coupling of ^{14}N is more sensitive to shear strains than to normal ones and according to the elastic tensor, the lattice is softer under shear stress. For the normal stress perpendicular to (111) , the stress can be decomposed to unit normal stress minus unit shear stress, and it results in a ring in Fig. 3(a) which has negative values. The eigenvalues and the eigenvectors of $dA_0/d\sigma$ can be found in Table I.

B. The temperature and pressure dependence of the static hyperfine interactions

To obtain the temperature and pressure dependence of the static hyperfine interaction, the free energy of diamond with an NV center $F(T, V)$ is calculated using Eq. (4) and fitted with the third-order Birch-Murnaghan equation [29], as shown in Fig. 2(a). The orange curve labeled “0 GPa” represents the equilibrium volume of $F(T, V)$ at $P = 0$, i.e.,

TABLE I. The eigenvalue and the eigenvector of the derivative of hyperfine parameter with respect to stress $\partial A_0/\partial \sigma$ (in units of kHz/GPa).

Nuclei	$\partial A_0/\partial \sigma$	eigenvector
^{14}N	12.3	(0.577, 0.579, 0.576)
	−6.7	(0.654, −0.750, 0.099)
	−6.6	(0.489, 0.320, −0.811)
$^{13}\text{C}(1)$	−492	(−0.424, 0.639, 0.642)
	104	(0.906, 0.297, 0.303)
	−29.0	(0.003, 0.710, −0.704)
$^{13}\text{C}(2)$	47.6	(1.000, −0.013, −0.027)
	−16.1	(0.028, 0.145, 0.989)
	−13.7	(0.009, 0.989, −0.145)
$^{13}\text{C}(3)$	19.0	(0.781, −0.439, −0.444)
	−0.1	(−0.625, −0.563, −0.541)
	3.6	(0.012, −0.700, 0.714)
$^{13}\text{C}(4)$	22.5	(−0.355, 0.661, 0.661)
	−17.9	(0.935, 0.252, 0.250)
	−11.4	(0.001, −0.707, 0.707)
$^{13}\text{C}(5)$	−30.5	(0.924, 0.013, 0.382)
	6.7	(−0.381, 0.104, 0.919)
	−3.9	(0.028, 0.995, −0.101)

$-\partial F(T, V)/\partial V = 0$, while the black dashed line labeled “classical” represents the equilibrium volume of total energy $E(0, V)$. These two curves differ even at $T = 0$ K because the former includes the effect of zero-point vibration, resulting in a 0.37% lattice expansion for diamond. Figure 2(b) shows the thermal expansion of diamond with an NV center, along with the experimental and calculated results for pristine diamond. The lattice with an NV center exhibits more noticeable thermal expansion compared to the pristine one, mainly due to the carbon vacancy. As shown in Figs. 2(b) and 2(c), the effect of temperature on volume change is insignificant at low thermal regimes, but becomes comparable to the effect of several gigapascals of hydrostatic compression at high temperatures of around or above 500 K. Our method is based on the harmonic approximation, which may not be valid at temperatures above 1000 K, where anharmonic effects become significant [45]. For a pressure change of 10 GPa, the variation in thermal expansion $\varepsilon(T, \sigma) - \varepsilon(0, \sigma)$ is much smaller than $\varepsilon(0, \sigma)$ itself. In Eq. (13), we consider the effect of $\varepsilon(0, \sigma) - \varepsilon_{\text{cls}}(\sigma)$ as $V(0, P) - V_{\text{cls}}(P)$, which is much easier to evaluate. Figure 2(d) shows a diagram of lattice expansions due to zero-point vibration. Unlike lattice variations under temperature and stress, the zero-point vibration part is quite stable over a wide range of pressures and has a value comparable to the effect of a negative pressure of approximately 4 GPa or thermal expansion at 1200 K.

In our previous work [20], we predicted the variation of the hyperfine parameter due to thermal expansion of lattice using $(dA_0/dV)[V_{\text{exp}}(T) - V_{\text{exp}}(0)]$, where the thermal expansion at $P = 0$ of the supercell with an NV center was approximated with the experimental data on perfect diamond $V_{\text{exp}}(T)$. In this work, we obtain the lattice expansion of the supercell with an NV center $V(T, P)$ via first-principles calculation, allowing us to discuss its temperature and pressure dependence based solely on first-principles calculations. The dA_0/V in Eq. (13) can be obtained by linear fitting of hyperfine interactions A_0 as a function of volumes V or lattice parameters.

The variation of the hyperfine tensor as a result of zero-point vibration $(dA_0/dV)[V(0, P) - V_{\text{cls}}(P)]$ via lattice shape change leads to a significant difference between hyperfine parameters $A_0(V(0, 0))$ and $A_0(V_{\text{cls}})$. As the temperature increases, the thermal expansion creating a deviation of $A_0(V(T, 0)) - A_0(V(0, 0))$ from zero. However, below 500 K, this term is much smaller than that due to zero-point vibration [see Figs. S4 and S5 in Ref. [43] for $A_0(V(T, P))$'s and their variations at finite temperature].

C. The vibrational contributions to hyperfine interactions and their volume dependence

The unitcell of diamond contains eight carbon atoms, so the pristine $4 \times 4 \times 4$ supercell contains 512 carbon atoms, and the supercell with a NV center, i.e., two neighboring carbons replaced by one N atom and one vacancy, contains $N_{\text{atom}} = 511$ atoms. The number of nonzero lattice vibration modes at Γ point is $3N_{\text{atom}} - 3 = 1530$, and these modes are indexed by $i = 1-1530$ in ascending order of phonon energy. To obtain the phonon-contributed hyperfine parameter at a specific volume, all the Γ -point vibration modes of the supercell are calculated in a range of lattices. To

estimate the influences of anharmonic vibrations (at fixed V) on hyperfine interaction, the perturbation $V' = \beta_i^{(3)} X_i^3$ is considered for any given mode i . The value $\beta_i^{(3)}$ is obtained by fitting the vibration potential $V(X_i)$. The first-order perturbation to the phonon wave function was considered, and then $\langle X_i \rangle_T$ is no longer zero but $-3\beta_i^{(3)} \hbar / \omega_i^3 (\langle n_i \rangle_T + 1/2)$. Hence, the tensor c_i in Eq. (12) was corrected by adding $b_i = -(3\hbar/2\omega_i^3)\beta_i^{(3)} dA_0/dX_i$. The first- and second-order derivative coefficients in respectively b_i and c_i were obtained by fitting the calculated data of $A_0(X_i)$ as quadratic functions of X_i , instead of using finite-difference in standard frozen-phonon method. The average phonon number at temperature T is $\langle n_i \rangle_T = [\exp(\hbar\omega_i/k_B T) - 1]^{-1}$. Calculations show that the b_i term is not important. Other anharmonic vibration terms such as $V'' = \beta_{ij}^{(3)} X_i X_j^2$ may also be considered. However, judging from the excellence of the quasiharmonic approximation to the equation of state parameters, all those terms are omitted in this calculation as they are extremely computationally costly. The quadratic fitting require a sufficiently large range of X_i to curb the influence of the numerical errors in $A_0(X_i)$, so that the accumulation of fitting errors in b_i , c_i do not ruin the results. The results presented in this work were based on an adaptive range of $\lesssim 1 \sqrt{\text{amu}} \text{ \AA}$ to curb the uncertainty due to the fluctuation of $A_0(X_i)$. “amu” here stands for the atomic mass unit, which is a unit of mass used to express the masses of atoms. $\sqrt{\text{amu}} \text{ \AA}$ here stands for the mass weighted displacement of atoms, which is the unit for canonical coordinates of vibrations.

The tensor c_i for the Fermi contact term is a scalar c_i and is plotted in Fig. 4, illustrating the contribution of each phonon mode to the hyperfine interaction on nuclei. The contribution due to b_i 's is about two or more orders of magnitude smaller (see Fig. S6 for the diagram of b_i similar to the form of c_i in Fig. 4). According to the phonon density of states, the number of phonon states are sparse at low frequencies, while these low frequency modes take the advantage of phonon number at the usual temperature up to about 1000 K. Figure 4 indicates that phonons with high-frequency is more important for $^{13}\text{C}(1-3)$ than $^{13}\text{C}(4-5)$ and ^{14}N , which is shown more clearly by the mode-accumulated contribution in Fig. S7. The anharmonic contributions are not important at room temperature since b_i are about two magnitudes smaller than the harmonic contributions c_i and mostly concentrate at high frequencies. Eq. (12) determines the $A_{\text{ph}}(T)$'s and their temperature derivatives for nuclei.

The vibrational contribution to the hyperfine tensor A_{ph} is a function of both temperature and pressure. In our previous work [20], this dependence was ignored by approximating $V(T, P) = V_{\text{cls}}$. As a result, the temperature dependence of hyperfine parameter variations and their temperature derivatives were approximately obtained with $A_0(V_{\text{exp}}(T)) + A_{\text{ph}}(T, V_{\text{cls}})$ (see Figs. S8 and S9 in Ref. [43] for the approximated hyperfine parameter). To assess the accuracy of the approximation, we evaluate the volume dependence of A_{ph} by separately considering the volume dependence of phonon frequencies ω_i and second-order coefficients $\partial^2 A_0 / \partial X_i^2$. In practice, they are calculated for each phonon mode in a series of volumes, similar to the process of obtaining $V(T, P)$ with the equation of state for diamond. To circumvent the challenge

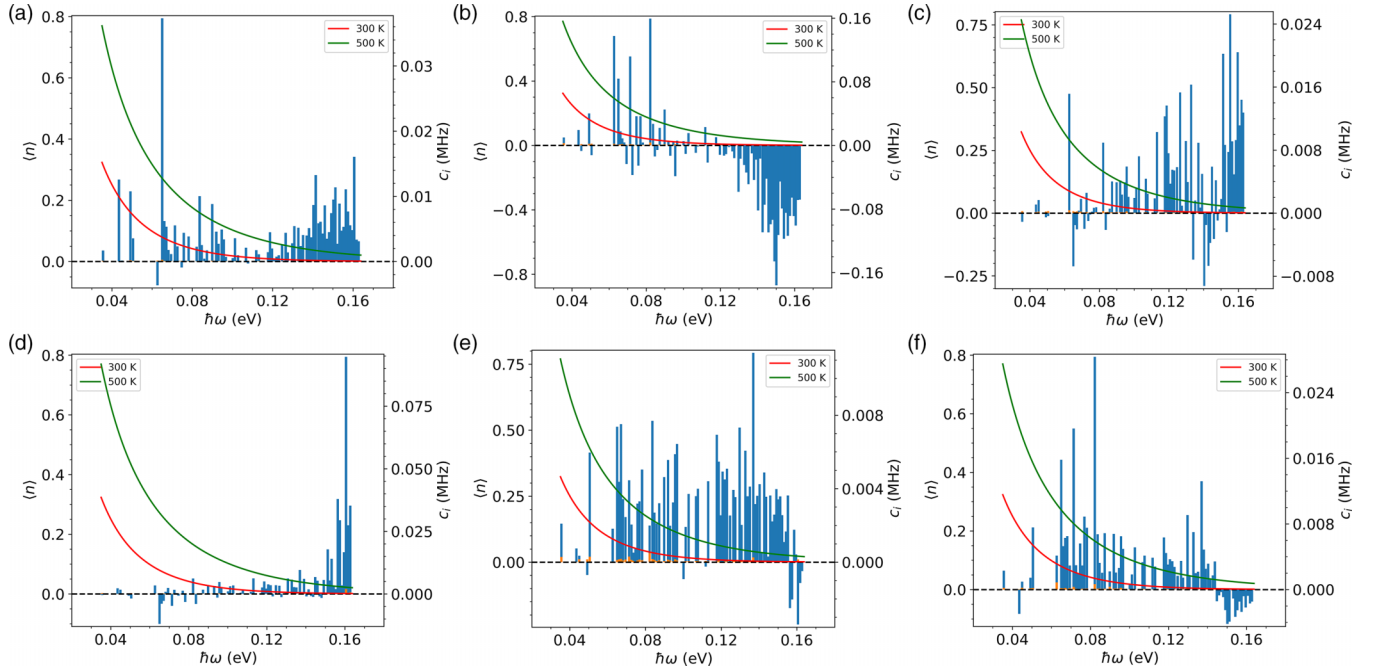


FIG. 4. The vibrational contribution per phonon on the Fermi contact term, i.e., c_i on (a) ^{14}N and [(b)–(f)] $^{13}\text{C}(1\text{--}5)$ with the phonon density of states and phonon number expectation at 300 K and $V_{\text{cls}}(0)$. The c_i parameters of near degenerate phonon modes in a range of 1 meV has been summed for purely illustrative purpose.

of matching phonon modes across different volumes during modewise calculations, we use the orthonormal atomic motions from the phonon calculations for $V_{\text{cls}}(0)$ across a series of volumes. Both phonon frequencies ω_i and second-order coefficients $\partial^2 A_0 / \partial X_i^2$ exhibit linear dependence on lattice parameters within a small range of volume. A_{ph} can then be obtained as a function of both temperature and pressure from Eq. (12). For all the nuclei we considered, the effects of volume dependence from second-order coefficients $\partial^2 A_0 / \partial X_i^2$ and phonon frequencies on A_{ph} are comparable. For ^{14}N , these effects nearly cancel out each other coincidentally, and make A_{ph} insensitive to volume changes (see Fig. S10 [43] for the effects of volume changes on A_{ph} via phonon frequencies and second-order coefficients).

The vibrational contribution to the hyperfine tensor variation A_{ph} can be separated into two parts calculated at the given $V(T, P)$: the zero-point vibrational contribution $A_{\text{ph}}(0, V(T, P))$ and finite-temperature part $A_{\text{ph}}(T, V(T, P)) - A_{\text{ph}}(0, V(T, P))$. The zero-point vibrational contribution can be further separated into the zero-point vibrational contribution at $V(0, P)$, i.e., $A_{\text{ph}}(0, V(0, P))$, and the part due to volume change, i.e., $A_{\text{ph}}(0, V(T, P)) - A_{\text{ph}}(0, V(0, P))$. These components of vibrational contribution to the hyperfine parameter of ^{14}N nucleus are presented in Fig. 5. As shown in Fig. 5(a), the zero-point vibrational contribution $A_{\text{ph}}(0, V(T, P))$ (calculated as change of A via Eq. (14), same below) is sensitive to pressure but insensitive to temperature via $V(T, P)$. The temperature dependence of $A_{\text{ph}}(T, V(T, P))$ in Fig. 5(d) is composed of the zero-point vibrational contribution in Fig. 5(b) and vibrational contribution in Fig. 5(c) at finite temperature. Comparisons among Figs. 5(a)–5(d) show that the zero-point vibrational contribution contributes more than that of the finite temperature

phonon to $A(T, P)$, as the phonon population of the majority modes at a temperature of interest is far less than $1/2$; while $A_{\text{ph}}(T, V(T, P)) - A_{\text{ph}}(0, V(T, P))$ contributes more to $\partial A / \partial T$ variation, since the phonon population $\langle n_i \rangle$ is strongly temperature dependent. The variation of $A_{\text{ph}}(0, V(T, P)) - A_{\text{ph}}(0, V(0, P))$ is two orders of magnitude smaller than $A_{\text{ph}}(T, V(T, P)) - A_{\text{ph}}(0, V(T, P))$, which indicates that the zero-point vibration has a negligible effect on $\partial A / \partial T$.

D. Hyperfine parameter as a function of thermal state variables

The temperature and pressure-dependent hyperfine parameter $A(T, P)$ for nuclei around an NV center was obtained by combining the volume-induced variation A_0 and the phonon-induced variation A_{ph} , as shown in Fig. 6. For these selected nuclei, the Fermi contact terms are dominant in hyperfine couplings (see Fig. S11 [43] for the comparison of Fermi contact term and hyperfine parameter for ^{14}N nucleus), and the Fermi contact term is a short-ranged interaction localized around the nuclei. Therefore these nuclei can be classified into two types according to their proximity to the high spin density region, as shown in Fig. 1. The first type includes ^{14}N , $^{13}\text{C}(4)$, and $^{13}\text{C}(5)$, which are not localized at the relatively flat spin density region; the second type includes $^{13}\text{C}(1)$, $^{13}\text{C}(2)$ and $^{13}\text{C}(3)$, which are localized at the high spin density region. As the phonon frequency increases, the nuclear motion $\langle X_i^2 \rangle_T$ decreases, which together with Fig. 4 may explain why the hyperfine interactions on ^{14}N , $^{13}\text{C}(4)$ and $^{13}\text{C}(5)$ nuclei are not sensitive to high-frequency phonon modes in the mode accumulated temperature derivative of the Fermi contact term $(\partial A_{\text{ph, Fermi}} / \partial T)|_{V_{\text{cls}}(0)}$ (see detailed mode accumulated temperature derivative of the Fermi contact term in Fig. S7 [43]). The Fermi contact term variations are small for the first type

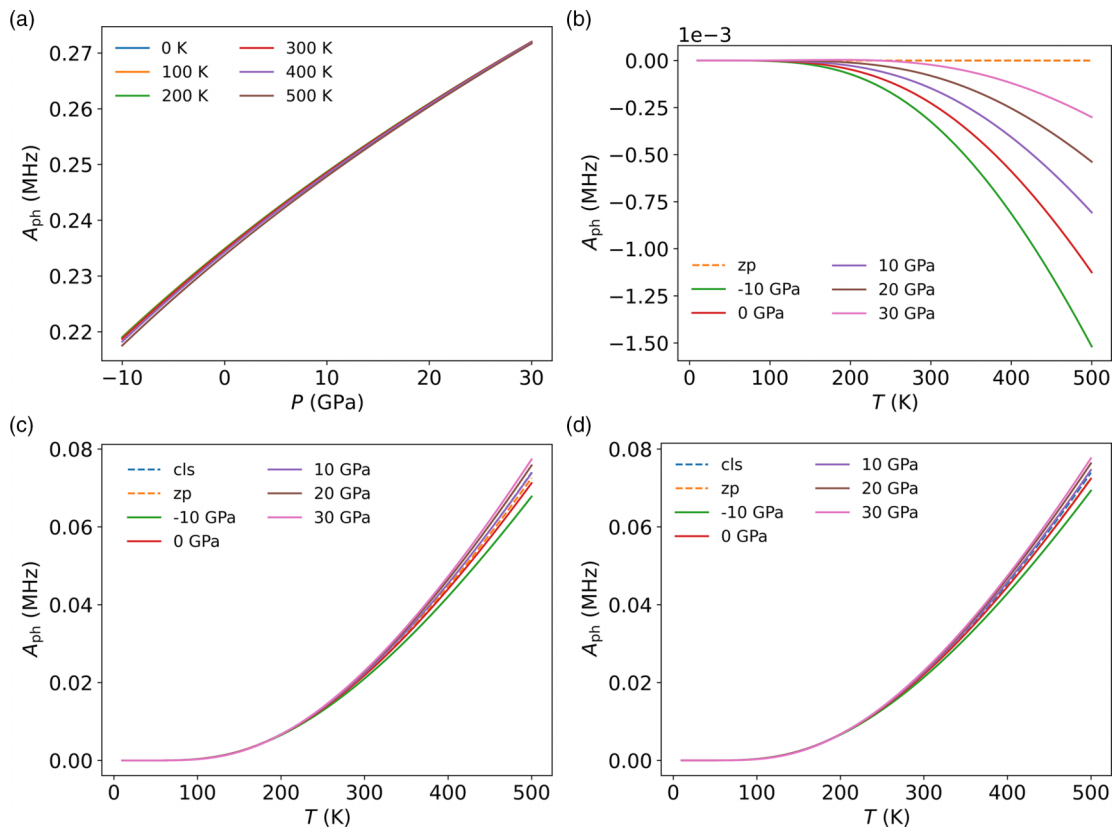


FIG. 5. The vibrational contribution to the hyperfine parameter of ^{14}N nucleus: (a) pressure dependence of zero-point vibrational contribution, $A_{\text{ph}}(0, V(T, P))$, (b) change in zero-point vibrational contribution due to thermal expansion, $A_{\text{ph}}(0, V(T, P)) - A_{\text{ph}}(0, V(0, P))$, (c) finite-temperature vibration part, $A_{\text{ph}}(T, V(T, P)) - A_{\text{ph}}(0, V(T, P))$, and (d) overall temperature dependence of vibrational contribution to hyperfine parameter under specific pressures, $A_{\text{ph}}(T, V(T, P)) - A_{\text{ph}}(0, V(0, P))$. Labels “cls” and “zp” in (b)–(d) represent results calculated in fixed volume $V_{\text{cls}}(0)$ and $V(0, 0)$, respectively.

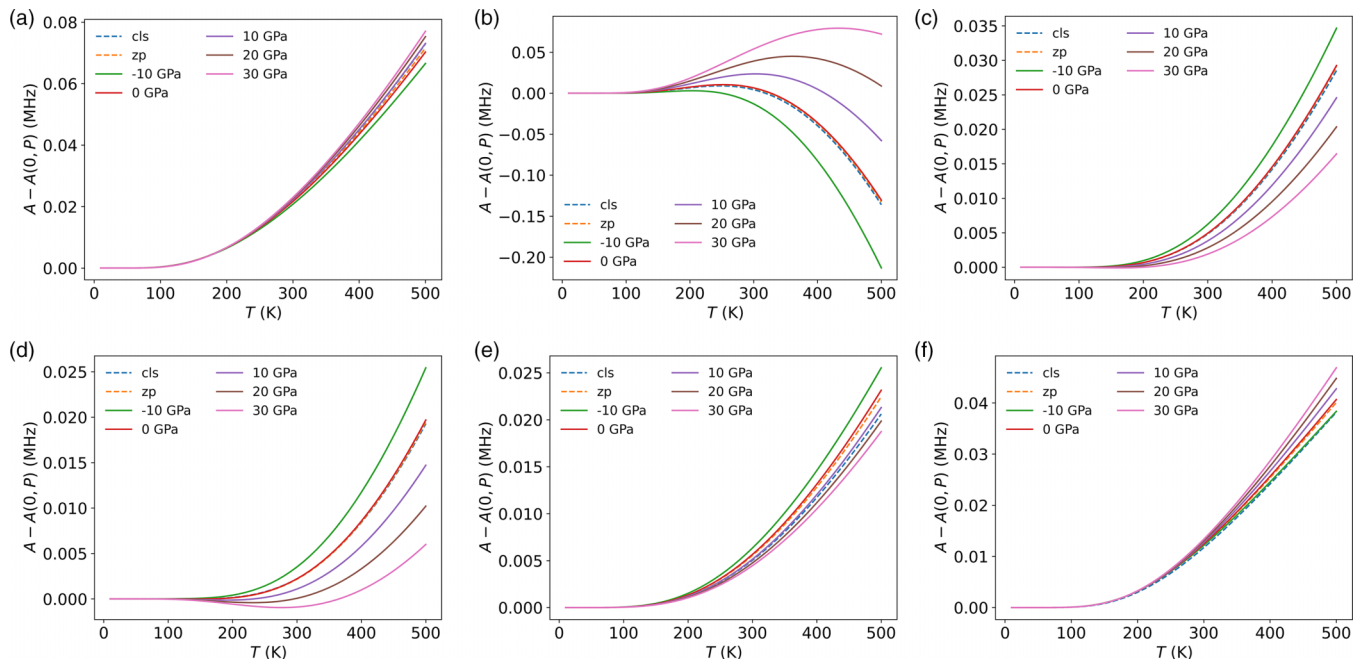


FIG. 6. Variation of hyperfine parameter $A(T, P) - A(0, P)$ with T under specific pressures for (a) ^{14}N and (b–f) $^{13}\text{C}(1-5)$ nuclei. Labels “cls” and “zp” represent results calculated in fixed volume $V_{\text{cls}}(0)$ and $V(0, 0)$.

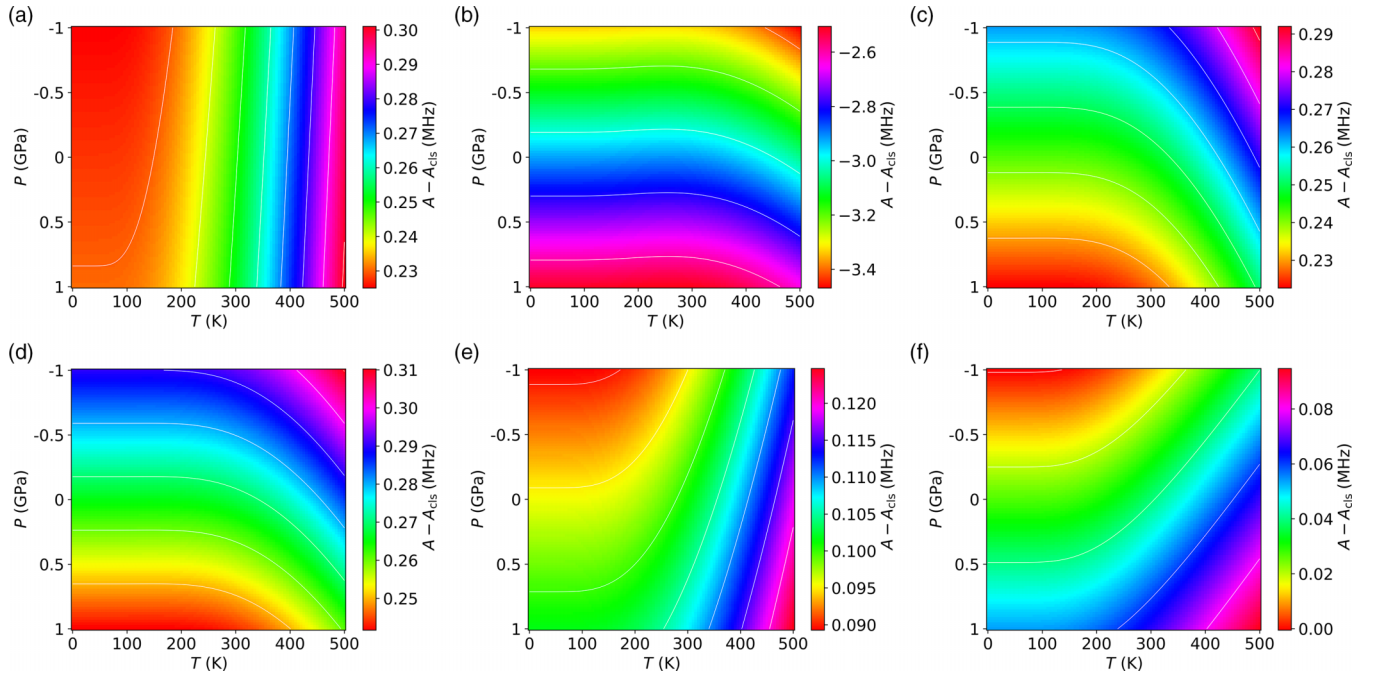


FIG. 7. Heatmap of hyperfine parameter $A(T, P)$ relative to $A_{\text{cls}} = A_0(V_{\text{cls}}(P = 0))$, i.e., $A(T, P) - A_{\text{cls}}$ of (a) ^{14}N and [(b)–(f)] $^{13}\text{C}(1\text{--}5)$ nuclei. The isolines are marked in white and their values are present in the ticks of the color bar on the right-hand side.

of nuclei and large for the others (the second type) when the lattice is under pressure or stress, so the second type of nuclei are more sensitive to pressure perturbation than the first type. We also calculate the temperature derivatives of $A(T, P)$ numerically for a variety of pressure P . The results at $V_{\text{cls}}(P)$ are calculated at fixed volumes and correspond to the results in our previous work [20] when $P = 0$. The comparison of results at $V_{\text{cls}}(P = 0)$ and $V(T = 0, P = 0)$ in Fig. 6 indicates that the effect of thermal expansion on the vibrational contribution is minimal. This confirms our previous approximate calculations, which were consistent with existing experimental data. We also found that the nuclei of the same type exhibit a similar pattern in their temperature derivatives. Detailed data on the temperature derivatives of $A(T, P)$ are included in Fig. S12 [43].

Figure 7 displays the contour plot of $A(T, P)$ within a pressure (stress) range of ± 1 GPa. The isolines illustrate how pressure affects the variation of the hyperfine parameter with temperature. Based on their patterns, nuclei can be divided into two distinct types: the hyperfine parameter of the ^{14}N nucleus in Fig. 7(a) primarily displays temperature dependence, while the hyperfine parameters of the $^{13}\text{C}(4)$ and $^{13}\text{C}(5)$ nuclei also exhibit noticeable temperature dependence. ^{14}N nucleus is a better choice for temperature sensors than $^{13}\text{C}(4)$ and $^{13}\text{C}(5)$, as its hyperfine parameter's temperature dependence is more resistant to pressure disturbances. Figure 7 also suggests that the ^{14}N nucleus may function down to a temperature of ~ 150 K, whereas the temperature window for $^{13}\text{C}(4)$ and $^{13}\text{C}(5)$ nuclei is narrower. Below room temperature, the hyperfine parameters of $^{13}\text{C}(1)$, $^{13}\text{C}(2)$, and $^{13}\text{C}(3)$ exhibit mainly pressure (stress) dependence at the level of ± 1 GPa. As higher temperatures, the temperature dependence of these hyperfine parameters becomes more pronounced.

When $A(T, P)$ is known, its second-order partial derivatives with respect to P and T can be calculated numerically, allowing us to measure how pressure affects $\partial A/\partial T$. For most nuclei, the relative variations of $\partial A/\partial T$ due to pressure $(\partial^2 A/\partial T \partial P)(\partial A/\partial T)^{-1}$ are on the order of $10^{-2}/\text{GPa}$ for most of the T - P ranges. Generally, relative variations are large at low temperatures and high pressures. The relative variation of $\partial A/\partial P$ due to unit temperature can be analyzed similarly. $\partial A/\partial P$ is far less affected by temperature in typical experimental environments, indicating that they can be treated independently (see Figs. S13 and S14 for details about the scales of relative variation of $\partial A/\partial T$ and $\partial A/\partial P$).

For ^{14}N , our calculated first and second temperature derivatives of the hyperfine parameters parallel (A_{\parallel}) and perpendicular (A_{\perp}) to the (111) direction at 300 K are 191.8 Hz/K and 0.71 Hz/K², and 132.9 Hz/K and 0.51 Hz/K², respectively, showing good agreement with experimental values for ^{14}N [46]. Table II summarizes the comparison (see Fig. S15 for the temperature derivatives of hyperfine parameters). The pressure derivatives of hyperfine param-

TABLE II. The hyperfine parameter A (in MHz), its temperature derivative dA/dT (in Hz/K) and the second derivative d^2A/dT^2 (in Hz/K²) of hyperfine parameters of ^{14}N parallel or perpendicular to (111) direction at 300 K. The experimental results are from Ref. [46].

	A_{\perp}		A_{\parallel}	
	calc	expt	calc	expt
A	-1.914	-2.635	-1.459	-2.165
dA/dT	132.9	154	191.8	197
d^2A/dT^2	0.51	0.53	0.71	0.73

ters are obtained in two ways: either by using the static approximation $dA_0(V_{\text{cls}}(P))/dP$, or by using the temperature and pressure dependent $A(T, P)$, i.e., $\partial A(T, P)/\partial P$ (see Table V and Fig. S16 for pressure derivatives of each nucleus). For $^{13}\text{C}(1)$, $dA_0(V_{\text{cls}}(P))/dP = 0.416$ MHz/GPa and $\partial A(T = 0, P)/\partial P = 0.406$ MHz/GPa are reasonably close to the measured value of 0.35 MHz/GPa reported in Ref. [47], considering we have not tried to optimize the calculation with more accurate functionals that would require more computational resources. Moreover, we calculate the temperature and pressure dependencies of the quadrupolar parameter [48] using the same approach as in calculating hyperfine couplings, while the nuclear quadrupole moment of ^{14}N is 20.44 millibarn [44]. Our result 28.46 Hz/K at 300 K agrees with the 35.0 Hz/K measured at 300 K in Ref. [20] (see Fig. S17 for the quadrupolar parameter results). Overall, our calculated results are in reasonably good agreement with existing experimental data, considering the fact that we did not specifically optimize the functional and pseudo-potential choices for the NV center system. Given that the PBE functional is known to exhibit delocalization errors that can affect the accuracy of hyperfine coupling [49], it may be worthwhile to consider and benchmark a more localized functional in future work to improve the accuracy of hyperfine coupling

IV. SUMMARY

The hyperfine interaction between the electron spin of the NV center in diamond and a surrounding nuclear spin is described with a tensor that is governed by the electron spin density distributions around the nucleus. The tensor at thermal equilibrium is treated as a macroscopic function of thermal variables and is calculated by introducing strains, thermal expansion, and lattice vibrations.

We calculated the hyperfine tensors' responses to a series of strains and found that they were linear within the range of interest. We then converted these responses to stress using an elastic tensor obtained from first-principles calculations. This linearity holds at typical stress levels up to at least several gigapascal. The temperature dependence of hyperfine coupling can be determined by considering both thermal expansion and vibrational contributions. The volume dependence that was previously overlooked in vibrational contributions is now included. The hyperfine tensor was calculated as a function of thermal state variables T and P using $V(T, P)$ obtained from first-principles calculations on supercell with NV center instead of the experimental thermal expansion function $V(T)$ of the pristine diamond at $P = 0$ GPa. It is worth mentioning that zero-point vibration contributes to the change in hyperfine tensors from its effect on equilibrium volume and distribution over the vibration coordinate. It has a non-negligible effect on the absolute value of hyperfine parameters but is not sensitive to changes in volume arising from temperature and pressure changes.

The hyperfine tensors of different nuclei have various sensitivities to lattice vibrations and external stress, reflecting the spatial distribution of electron spin density around the nuclei. Nuclei can be classified into two categories based on their onsite electron spin density. The hyperfine parameters of carbon nuclei $^{13}\text{C}(1-3)$, which locate in regions with

relatively high spin density, have a variation with temperature that is more susceptible to stress disturbances, while other nuclei studied, ^{14}N and $^{13}\text{C}(4-5)$, exhibit more stable temperature dependence that is less perturbed by stress. For the ^{14}N nucleus, variation in hyperfine interaction is mainly due to the vibrational contribution A_{ph} . The two volume-dependent effects on the vibrational contribution almost cancel out each other, rendering the hyperfine parameter of the ^{14}N nucleus insensitive to volume changes. For all the surrounding ^{13}C nuclei, our calculations confirm previous findings that both thermal expansion and vibrational contributions are significant.

The calculated hyperfine interactions as functions of temperature and pressure were validated by comparing various temperature or pressure derivatives with available experimental data. Our results reveal a complex interplay among the structural, vibrational and spin properties of the NV center system and provide a comprehensive method for calculating small variations of physical quantities due to external perturbations.

ACKNOWLEDGMENTS

This work was supported by Innovation Program for Quantum Science and Technology (Grants No. 2021ZD0302200 and No. 2021ZD0303204), the National Key R&D Program of China (Grant No. 2018YFA0306600), the National Natural Science Foundation of China (Grants No. T2125011 and No. 12274396), the CAS (Grants No. GJJSTD20200001 and No. Y201984), the Anhui Initiative in Quantum Information Technologies (Grant No. AHY050000), the CAS Project for Young Scientists in Basic Research, the Fundamental Research Funds for the Central Universities, and the China Postdoctoral Science Foundation (Grants No. 2021M703110 and No. 2022T150631). Numerical calculations were carried out on the supercomputing system at the Supercomputing Center of the University of Science and Technology of China.

APPENDIX A: THE HYPERFINE TENSORS AT THE STATIC CONFIGURATION MINIMIZING THE TOTAL ENERGY

The hyperfine tensors calculated at the static configuration that minimize the total energy of the E_{grd} are listed in units of MHz as follows:

$$A(^{14}\text{N}) = \begin{pmatrix} -1.9639 & 0.13506 & 0.13521 \\ 0.13506 & -1.9641 & 0.13515 \\ 0.13521 & 0.13515 & -1.9638 \end{pmatrix}, \quad (\text{A1})$$

$$A(^{13}\text{C}(1)) = \begin{pmatrix} 146.84 & -27.499 & -27.499 \\ -27.499 & 144.32 & 26.095 \\ -27.499 & 26.095 & 144.32 \end{pmatrix}, \quad (\text{A2})$$

TABLE III. The independent elements of elastic tensor of diamond with an NV center in Eq. (B1) obtained at V_{cls} .

element	C_{11}	C_{12}	C_{44}	C_{45}	C_{15}	C_{14}
value (GPa)	1081.0(8)	151(2)	593(3)	-0.01(8)	0.14(9)	0.08(6)

TABLE IV. The strain derivative of hyperfine tensor $\partial A_0/\partial \varepsilon$ (in units of MHz) under normal strains, shear strains and the relative variation of lattice parameter $\delta L/L$, i.e. $\varepsilon_{xx} = \varepsilon_{yy} = \varepsilon_{zz} = \delta L/L$.

strain	^{14}N	$^{13}\text{C}(1)$	$^{13}\text{C}(2)$	$^{13}\text{C}(3)$	$^{13}\text{C}(4)$	$^{13}\text{C}(5)$
ε_{xx}	-0.5(6)	-66(4)	46.9(3)	14.1(5)	-12.9(1)	-27.6(3)
ε_{yy}	-0.5(6)	-255(3)	-10.1(4)	8.4(3)	1.7(1)	-7.7(2)
ε_{zz}	-0.5(6)	-256(3)	-12.2(3)	8.5(3)	1.7(1)	-3.2(2)
$\delta L/L$	-1.6(1)	-517(5)	24.8(2)	30.2(2)	-8.6(1)	-34.7(3)
ε_{xy}	7.5(1)	191(4)	-1.0(4)	-7.8(3)	-11.2(1)	-0.9(3)
ε_{yz}	7.4(1)	193(4)	-2.0(3)	-7.8(3)	-11.2(1)	-15.5(3)
ε_{zx}	7.5(1)	-211(2)	-0.4(3)	2.3(3)	17.1(2)	1.0(3)

$$A(^{13}\text{C}(2)) = \begin{pmatrix} 16.204 & -1.9033 & -2.0577 \\ -1.9033 & 16.075 & 1.8803 \\ -2.0577 & 1.8803 & 16.119 \end{pmatrix}, \quad (\text{A3})$$

$$A(^{13}\text{C}(3)) = \begin{pmatrix} 14.893 & -1.7933 & -1.7932 \\ -1.7933 & 14.914 & 1.9352 \\ -1.7932 & 1.9352 & 14.914 \end{pmatrix}, \quad (\text{A4})$$

$$A(^{13}\text{C}(4)) = \begin{pmatrix} -8.4564 & 0.1931 & 0.1930 \\ 0.1931 & -7.7301 & 1.1128 \\ 0.1930 & 1.1128 & -7.7305 \end{pmatrix}, \quad (\text{A5})$$

$$A(^{13}\text{C}(5)) = \begin{pmatrix} -4.305 & 0.8166 & -1.3614 \\ 0.8166 & -4.773 & -0.9158 \\ -1.3614 & -0.9158 & -4.691 \end{pmatrix}. \quad (\text{A6})$$

APPENDIX B: THE ELASTIC TENSOR RESTRICTED BY SYMMETRY

Both stress σ and strain ε are symmetric rank-2 tensors with six independent components. Due to the symmetry of

TABLE V. The pressure derivatives of hyperfine parameter $-\frac{\partial A_0}{\partial P} = \frac{\partial A_0}{\partial \sigma_{xx}} + \frac{\partial A_0}{\partial \sigma_{yy}} + \frac{\partial A_0}{\partial \sigma_{zz}}$ obtained at V_{cls} (in units of MHz/GPa).

nucleus	^{14}N	$^{13}\text{C}(1)$	$^{13}\text{C}(2)$	$^{13}\text{C}(3)$	$^{13}\text{C}(4)$	$^{13}\text{C}(5)$
$\partial A_0/\partial P$	1.1×10^{-3}	0.416	-0.0177	-0.0224	6.85×10^{-3}	0.0277

the NV center being described by the point group C_{3v} , the number of independent modulus components relating stress σ to strain ε is reduced from 21 to 6, which are given as follows:

$$\begin{pmatrix} \sigma_{xx} \\ \sigma_{yy} \\ \sigma_{zz} \\ \sigma_{yz} \\ \sigma_{xz} \\ \sigma_{xy} \end{pmatrix} = \begin{pmatrix} C_{11} & C_{12} & C_{12} & C_{14} & C_{15} & C_{14} \\ C_{12} & C_{11} & C_{12} & C_{14} & C_{14} & C_{15} \\ C_{12} & C_{12} & C_{11} & C_{15} & C_{14} & C_{14} \\ C_{14} & C_{14} & C_{15} & C_{44} & C_{45} & C_{45} \\ C_{15} & C_{14} & C_{14} & C_{45} & C_{44} & C_{45} \\ C_{14} & C_{15} & C_{14} & C_{45} & C_{45} & C_{44} \end{pmatrix} \begin{pmatrix} \varepsilon_{xx} \\ \varepsilon_{yy} \\ \varepsilon_{zz} \\ 2\varepsilon_{yz} \\ 2\varepsilon_{xz} \\ 2\varepsilon_{xy} \end{pmatrix}. \quad (\text{B1})$$

Their values are listed in Table III. For the pristine diamond, the high crystallographic point group O_h restricts the elements C_{45} , C_{15} and C_{14} in the elastic tensor to be strictly zero.

APPENDIX C: THE STRAIN AND STRESS DEPENDENCE OF THE HYPERFINE PARAMETERS

The strain and stress derivatives of the hyperfine parameters, $\partial A_0/\partial \varepsilon$, are listed in Tables IV and V, respectively.

- [1] G. Wolfowicz, F. J. Heremans, C. P. Anderson, S. Kanai, H. Seo, A. Gali, G. Galli, and D. D. Awschalom, Quantum guidelines for solid-state spin defects, *Nat. Rev. Mater.* **6**, 906 (2021).
- [2] C. L. Degen, F. Reinhard, and P. Cappellaro, Quantum sensing, *Rev. Mod. Phys.* **89**, 035002 (2017).
- [3] D. D. Awschalom, R. Hanson, J. Wrachtrup, and B. B. Zhou, Quantum technologies with optically interfaced solid-state spins, *Nat. Photon.* **12**, 516 (2018).
- [4] M. W. Doherty, N. B. Manson, P. Delaney, F. Jelezko, J. Wrachtrup, and L. C. L. Hollenberg, The nitrogen-vacancy colour centre in diamond, *Phys. Rep.* **528**, 1 (2013).
- [5] F. Shi, Q. Zhang, P. Wang, H. Sun, J. Wang, X. Rong, M. Chen, C. Ju, F. Reinhard, H. Chen *et al.*, Single-protein spin resonance spectroscopy under ambient conditions, *Science* **347**, 1135 (2015).
- [6] I. Lovchinsky, A. O. Sushkov, E. Urbach, N. P. de Leon, S. Choi, K. De Greve, R. Evans, R. Gertner, E. Bersin, C. Müller *et al.*, Nuclear magnetic resonance detection and spectroscopy of single proteins using quantum logic, *Science* **351**, 836 (2016).
- [7] F. Shi, F. Kong, P. Zhao, X. Zhang, M. Chen, S. Chen, Q. Zhang, M. Wang, X. Ye, Z. Wang *et al.*, Single-DNA electron spin resonance spectroscopy in aqueous solutions, *Nat. Methods* **15**, 697 (2018).
- [8] L. Thiel, Z. Wang, M. A. Tschudin, D. Rohner, I. Gutiérrez-Lezama, N. Ubrig, M. Gibertini, E. Giannini, A. F. Morpurgo, and P. Maletinsky, Probing magnetism in 2D materials at the nanoscale with single-spin microscopy, *Science* **364**, 973 (2019).
- [9] M. J. H. Ku, T. X. Zhou, Q. Li, Y. J. Shin, J. K. Shi, C. Burch, L. E. Anderson, A. T. Pierce, Y. Xie, A. Hamo *et al.*, Imaging viscous flow of the Dirac fluid in graphene, *Nature (London)* **583**, 537 (2020).
- [10] T. Song, Q.-C. Sun, E. Anderson, C. Wang, J. Qian, T. Taniguchi, K. Watanabe, M. A. McGuire, R. Stöhr, D. Xiao *et al.*, Direct visualization of magnetic domains and moiré magnetism in twisted 2D magnets, *Science* **374**, 1140 (2021).
- [11] G. Kucsko, P. C. Maurer, N. Y. Yao, M. Kubo, H. J. Noh, P. K. Lo, H. Park, and M. D. Lukin, Nanometrescale thermometry in a living cell, *Nature (London)* **500**, 54 (2013).
- [12] P. Neumann, I. Jakobi, F. Dolde, C. Burk, R. Reuter, G. Waldherr, J. Honert, T. Wolf, A. Brunner, J. H. Shim, D. Suter, H. Sumiya, J. Isoya, and J. Wrachtrup, High-precision

- nanoscale temperature sensing using single defects in diamond, *Nano Lett.* **13**, 2738 (2013).
- [13] M. Pompili, S. L. N. Hermans, S. Baier, H. K. C. Beukers, P. C. Humphreys, R. N. Schouten, R. F. L. Vermeulen, M. J. Tiggelman, L. dos Santos Martins, B. Dirkse *et al.*, Realization of a multinode quantum network of remote solid-state qubits, *Science* **372**, 259 (2021).
- [14] S. L. N. Hermans, M. Pompili, H. K. C. Beukers, S. Baier, J. Borregaard, and R. Hanson, Qubit teleportation between non-neighbouring nodes in a quantum network, *Nature (London)* **605**, 663 (2022).
- [15] D. A. Simpson, E. Morrisroe, J. M. McCoe, A. H. Lombard, D. C. Mendis, F. Treussart, L. T. Hall, S. Petrou, and L. C. L. Hollenberg, Non-neurotoxic nanodiamond probes for intraneuronal temperature mapping, *ACS Nano* **11**, 12077 (2017).
- [16] P. Udvarhelyi, V. O. Shkolnikov, A. Gali, G. Burkard, and A. Pályi, Spin-strain interaction in nitrogen-vacancy centers in diamond, *Phys. Rev. B* **98**, 075201 (2018).
- [17] V. Ivády, T. Simon, J. R. Maze, I. A. Abrikosov, and A. Gali, Pressure and temperature dependence of the zero-field splitting in the ground state of nv centers in diamond: A first-principles study, *Phys. Rev. B* **90**, 235205 (2014).
- [18] Y. Yang, H. H. Vallabhapurapu, V. K. Sewani, M. Isarov, H. R. Firgau, C. Adambukulam, B. C. Johnson, J. J. Pla, and A. Laucht, Observing hyperfine interactions of nv- centers in diamond in an advanced quantum teaching lab, *Am. J. Phys.* **90**, 550 (2022).
- [19] S. Felton, A. M. Edmonds, M. E. Newton, P. M. Martineau, D. Fisher, D. J. Twitchen, and J. M. Baker, Hyperfine interaction in the ground state of the negatively charged nitrogen vacancy center in diamond, *Phys. Rev. B* **79**, 075203 (2009).
- [20] S. Xu, M. Liu, T. Xie, Z. Zhao, Q. Shi, P. Yu, C.-K. Duan, F. Shi, and J. Du, High-precision measurements and first-principles explanation of the temperature-dependent ^{13}C and ^{14}N hyperfine interactions of single nv^- centers in diamond at room temperature, *Phys. Rev. B* **107**, L140101 (2023).
- [21] H. Tang, A. R. Barr, G. Wang, P. Cappellaro, and J. Li, First-principles calculation of the temperature-dependent transition energies in spin defects, *J. Phys. Chem. Lett.* **14**, 3266 (2023).
- [22] B. T. Sutcliffe, The born-oppenheimer approximation, in *Methods in Computational Molecular Physics*, edited by S. Wilson and G. H. F. Dierksen (Springer US, Boston, MA, 1992), pp. 19–46.
- [23] P. E. Blöchl, First-principles calculations of defects in oxygen-deficient silica exposed to hydrogen, *Phys. Rev. B* **62**, 6158 (2000).
- [24] S. Blügel, H. Akai, R. Zeller, and P. H. Dederichs, Hyperfine fields of 3d and 4d impurities in nickel, *Phys. Rev. B* **35**, 3271 (1987).
- [25] O. V. Yazyev, I. Tavernelli, L. Helm, and U. Röthlisberger, Core spin-polarization correction in pseudopotential-based electronic structure calculations, *Phys. Rev. B* **71**, 115110 (2005).
- [26] X. Zhang, B. Grabowski, T. Hickel, and J. Neugebauer, Calculating free energies of point defects from ab initio, *Comput. Mater. Sci.* **148**, 249 (2018).
- [27] D. Murali, M. Posselt, and M. Schiwarth, First-principles calculation of defect free energies: General aspects illustrated in the case of bcc Fe, *Phys. Rev. B* **92**, 064103 (2015).
- [28] A. Togo and I. Tanaka, First principles phonon calculations in materials science, *Scr. Mater.* **108**, 1 (2015).
- [29] P. Vinet, J. H. Rose, J. Ferrante, and J. R. Smith, Universal features of the equation of state of solids, *J. Phys.: Condens. Matter.* **1**, 1941 (1989).
- [30] P. Jacobson and S. Stoupin, Thermal expansion coefficient of diamond in a wide temperature range, *Diam. Relat. Mater.* **97**, 107469 (2019).
- [31] https://www.vasp.at/wiki/index.php/Phonons_from_finite_differences#cite_ref-wu:prb:2005_2-0.
- [32] F. Giustino, Electron-phonon interactions from first principles, *Rev. Mod. Phys.* **89**, 015003 (2017).
- [33] P. E. Blöchl, Projector augmented-wave method, *Phys. Rev. B* **50**, 17953 (1994).
- [34] G. Kresse and J. Hafner, Ab initio molecular dynamics for liquid metals, *Phys. Rev. B* **47**, 558 (1993).
- [35] G. Kresse and J. Hafner, Ab initio molecular-dynamics simulation of the liquid-metal–amorphous-semiconductor transition in germanium, *Phys. Rev. B* **49**, 14251 (1994).
- [36] J. P. Perdew, A. Ruzsinszky, G. I. Csonka, O. A. Vydrov, G. E. Scuseria, L. A. Constantin, X. Zhou, and K. Burke, Restoring the density-gradient expansion for exchange in solids and surfaces, *Phys. Rev. Lett.* **100**, 136406 (2008).
- [37] https://www.vasp.at/wiki/index.php/Energy_vs_volume_Volume_relaxations_and_Pulay_stress.
- [38] http://nmrwiki.org/wiki/index.php?title=Gyromagnetic_ratio.
- [39] G. D. Mahan, Effect of atomic isotopes on phonon modes, *Phys. Rev. B* **100**, 024307 (2019).
- [40] P. G. Klemens, The scattering of low-frequency lattice waves by static imperfections, *Proc. Phys. Soc. A* **68**, 1113 (1955).
- [41] O. A. Bauchau and J. I. Craig, eds., *Structural Analysis* (Springer Netherlands, 2009).
- [42] H. J. McSkimin and P. Andreatch, Elastic moduli of diamond as a function of pressure and temperature, *J. Appl. Phys.* **43**, 2944 (1972).
- [43] See Supplemental Material at <http://link.aps.org/supplemental/10.1103/PhysRevB.108.155150> for additional details on the impact of stress and lattice vibration on hyperfine interactions.
- [44] P. Pyykkö, Year-2008 nuclear quadrupole moments, *Mol. Phys.* **106**, 1965 (2008).
- [45] T. A. Ivanova and B. N. Mavrin, *Ab initio* temperature dependence of the thermal expansion of diamond and the frequency shift of optical phonons, *Phys. Solid State* **55**, 160 (2013).
- [46] S. Lourette, A. Jarmola, V. M. Acosta, A. G. Birdwell, D. Budker, M. W. Doherty, T. Ivanov, and V. S. Malinovsky, Temperature sensitivity of ^{14}NV and ^{15}NV ground state manifolds, *Phys. Rev. Appl.* **19**, 064084 (2023).
- [47] K. O. Ho, M. Y. Leung, P. Reddy, J. Xie, K. C. Wong, Y. Jiang, W. Zhang, K. Y. Yip, W. K. Leung, Y. Y. Pang, K. Y. Yu, S. K. Goh, M. W. Doherty, and S. Yang, Probing the evolution of the electron spin wave function of the nitrogen-vacancy center in diamond via pressure tuning, *Phys. Rev. Appl.* **18**, 064042 (2022).
- [48] H. M. Petrilli, P. E. Blöchl, P. Blaha, and K. Schwarz, Electric-field-gradient calculations using the projector augmented wave method, *Phys. Rev. B* **57**, 14690 (1998).
- [49] K. Szász, T. Hornos, M. Marsman, and A. Gali, Hyperfine coupling of point defects in semiconductors by hybrid density functional calculations: The role of core spin polarization, *Phys. Rev. B* **88**, 075202 (2013).